# GFMC calculations of electromagnetic moments and M1 transitions in $A \leq 9$ nuclei

**S. Pastore**[*]
*Department of Physics and Astronomy, University of South Carolina, Columbia, SC 29208*
*E-mail:* `pastores@mailbox.sc.edu`

**Steven C. Pieper**
*Physics Division, Argonne National Laboratory, Argonne, Illinois 60439*
*E-mail:* `spieper@anl.gov`

**R. Schiavilla**
*Theory Center, Jefferson Laboratory, Newport News, Virginia 23606,*
*Department of Physics, Old Dominion University, Norfolk, Virginia 23529*
*E-mail:* `schiavil@jlab.org`

**R. B. Wiringa**
*Physics Division, Argonne National Laboratory, Argonne, Illinois 60439*
*E-mail:* `wiringa@anl.gov`

We present recent Green's function Monte Carlo calculations of magnetic moments and M1 transitions in $A \leq 9$ nuclei, which include corrections arising from two-body meson-exchange electromagnetic currents. Two-body effects provide significant corrections to the calculated observables, bringing them in excellent agreement with the experimental data. In particular, we find that two-body corrections are especially large in the $A = 9$, $T = 3/2$ systems, in which they account for up to $\sim 20\%$ ($\sim 40\%$) of the total predicted value for the $^9$Li ($^9$C) magnetic moment.
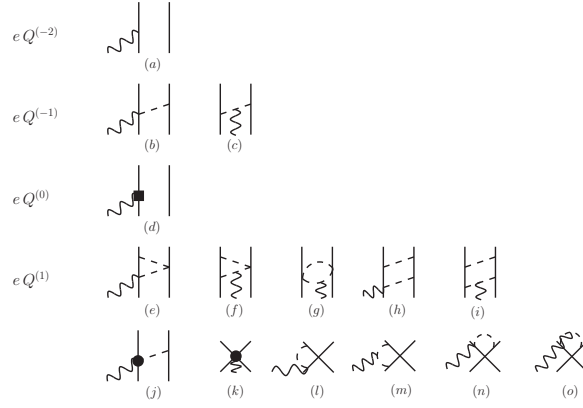
[*]Speaker.

**Figure 1:** Diagrams illustrating one- and two-body $\chi$EFT EM currents entering at LO ($eQ^{-2}$), NLO ($eQ^{-1}$), N2LO ($eQ^0$), and N3LO ($eQ^1$). Nucleons, pions, and photons are denoted by solid, dashed, and wavy lines, respectively.

In this contribution, we present a set of Green's function Monte Carlo (GFMC) calculations of magnetic moments (m.m.'s) and M1 transitions in $A \leq 9$ nuclei, which has been recently reported in Ref. [1]. In these calculations, nuclear wave functions (w.f.'s) are constructed from a Hamiltonian consisting of the Argonne-$v_{18}$ two-nucleon [2] and Illinois-7 three-nucleon potentials [3], with which the computed GFMC ground- and excited-state energies are found to be in good agreement with experiments [1]. The electromagnetic (EM) current operator includes, in addition to the standard one-body convection and spin-magnetization terms for individual protons and neutrons, a two-body meson-exchange-current (MEC) component. The latter is constructed within two distinct frameworks, namely the standard nuclear physics approach (SNPA) illustrated in Refs. [4, 5], and the pionfull chiral effective field theory ($\chi$EFT) formulation of Refs. [6, 7, 8]. In what follows, we summarize on the methods and results discussed in Ref. [1].

## 1. GFMC Method and the Nuclear Hamiltonian

The EM transition matrix elements are evaluated in between w.f.'s which are solutions of the Schrödinger equation, with a nuclear Hamiltonian, H, consisting of a kinetic term plus two- and three-body interaction terms—in the present case, the Argonne-$v_{18}$ and Illinois-7, respectively. Nuclear w.f.'s are constructed in two steps. First, a trial variational Monte Carlo w.f. ($\Psi_T$), which accounts for the effect of the nuclear interaction via the inclusion of correlation operators, is generated by minimizing the energy expectation value with respect to a number of variational parameters. The second step improves on $\Psi_T$ by eliminating excited states contamination. This is accomplished by the GFMC calculation which propagates the Schrödinger equation in imaginary time ($\tau$). The propagated w.f. $\Psi(\tau) = e^{-(H-E_0)\tau}\Psi_T$, for large values of $\tau$, converges to the exact w.f. with eigenvalue $E_0$. Ideally, the matrix elements should be evaluated in between two propagated w.f.'s. In practice, we evaluate mixed estimates in which only one w.f. is propagated, while the remaining one is replaced by $\Psi_T$. The calculation of diagonal and off-diagonal matrix elements is discussed at length in Ref. [9] and references therein.

2

The nuclear EM current operator is also expressed as an expansion in many-body operators. The current utilized in the calculations accounts up to two-body effects, and is written as:

$$\mathbf{j}(\mathbf{q}) = \sum_i \mathbf{j}_i(\mathbf{q}) + \sum_{i<j} \mathbf{j}_{ij}(\mathbf{q}) \,, \tag{1.1}$$

where $\mathbf{q}$ is the momentum associated with the external EM field. The one-body operator at leading order, *i.e.* the impulse approximation (IA) operator, consists of the convection and the spin-magnetization currents associated with an individual nucleon [1], and it is diagrammatically represented in panel (a) of Fig. 1.

## 2. $\chi$EFT and SNPA EM currents

In the calculations, two models for the EM two-body MEC operators are tested, namely the pionful $\chi$EFT and SNPA models. The $\chi$EFT current operators are expanded in powers of pions' and nucleons' momenta, $Q$, and consist of long- and intermediate-range components which are described in terms of one- and two-pion exchange contributions, as well as contact currents which encode the short-range physics. These operators involve a number of Low Energy Constants (LECs) which are then fixed to the experimental data. Currents from pionful $\chi$EFT including up to two-pion exchange contributions were derived originally by Park, Min, and Rho in covariant perturbation theory [10]. More recently, Kölling and collaborators presented EM currents obtained within the method of unitary transformations [11, 12]. Here, we refer to the EM operators constructed in Ref. [6, 7, 8], in which time-ordered perturbation theory is implemented to calculate the EM transition amplitudes. These EM operators are diagrammatically represented in Fig. 1, where they are listed according to their scaling in $eQ$, (where $e$ is the electric charge).

Referring to this figure, one-body contributions enter at LO, panel (a), and N2LO, panel (d), and they are the IA current operator at LO and its relativistic correction, respectively. The NLO term involves seagull and in-flight long-range contributions associated with one-pion exchange (OPE). At N3LO we include the two-pion-range contributions of diagrams (e)–(i), the one-pion-range tree-level current involving a $\gamma\pi NN$ vertex of order $eQ^2$, diagram (j), the contact currents of diagram (k), as well as the one-loop corrections of diagrams (l)–(o). The two-body operators have a power-law behavior at large momenta, therefore a regularization procedure is implemented via the introduction of cutoff function of the form $exp(-Q^4/\Lambda^4)$ [8], where $\Lambda = 600$ MeV.

The contact currents of diagram (k) are of minimal and non-minimal nature. The former are linked to the $\chi$EFT potential at order $Q^2$ via current conservation; therefore they involve the same LECs entering the $\chi$EFT NN interaction, and can be taken from fits to the NN scattering data. We use the values obtained from the analysis of Refs. [16], with cutoff $\Lambda = 600$ MeV. Non-minimal LECs entering the contact and tree-level currents at N3LO—diagrams (j) and (k), respectively— need to be fixed to EM observables. The fitting procedure has been implemented by Piarulli *et al.* in Ref. [8]. In that work, LECs multiplying isovector operators in the tree-level current are fixed by saturating the $\Delta$-resonance [10] (a common strategy adopted, for example, in Refs. [13, 14, 15]). The remaining three LECs are fixed so as to reproduce the deuteron, $^3$He, and $^3$H m.m.'s.

The second model for the EM MEC operators utilized in the calculations is the SNPA model. Two-body currents in the SNPA formalism, described at length in Refs. [4, 5] and references
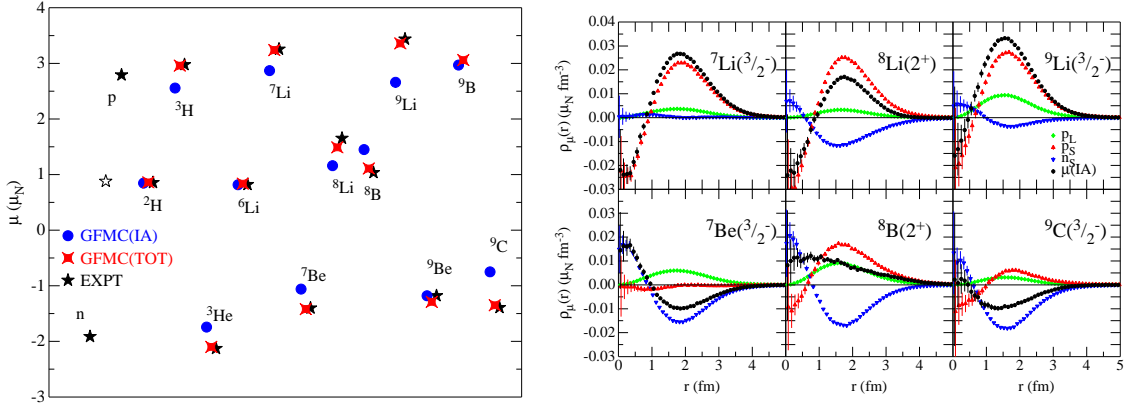
**Figure 2: Left**: Magnetic moments in nuclear magnetons for $A \leq 9$ nuclei. Black stars indicate the experimental values [17, 18], while blue dots (red diamonds) represent preliminary GFMC calculations which include the IA one-body EM current (full $\chi$EFT current up to N3LO). Predictions are for nuclei with $A > 3$. **Right**: Magnetic density in nuclear magnetons per fm$^3$ for selected nuclei, including only the IA current contribution.

therein, are separated into model-independent (MI) and model-dependent (MD) terms. The former (MI) are derived from the *NN* potential, and their longitudinal components satisfy, by construction, current conservation with it, thus their short-range behavior is consistent with that of the potential. The dominant terms, isovector in character, originate from the static part of the potential, which is assumed to be due to exchanges of effective pseudoscalar (PS or "$\pi$-like") and vector (PV or "$\rho$-like") mesons. The associated currents are then constructed by using the PS and PV propagators, projected out of the static potential [4]. At large inter-nucleon separations, where the *NN* potential is driven by the OPE mechanism, the MI current coincides with the standard seagull and pion-in-flight OPE currents diagrammatically illustrated in panels (b) and (c), respectively, of Fig. 1. The MD currents are purely transverse, and unconstrained by current conservation. The dominant term is associated with excitation of intermediate $\Delta$ isobars. Additional and small MD currents arise from the isoscalar $\rho\pi\gamma$ and isovector $\omega\pi\gamma$ transition mechanisms [4, 5].

## 3. Results

Results for the m.m.'s of $A \leq 9$ nuclei indicate that two-body MEC corrections evaluated in both the SNPA and $\chi$EFT models are qualitatively in agreement, and, when large, they boost the IA in the direction of the experimental data. We summarize the m.m.'s calculations in the left panel of Fig. 2, where we show the results obtained with the $\chi$EFT model. In this figure, black stars represent the experimental data [17, 18]—there are no data for the m.m. of $^9$B.[1] For completeness, we show also the experimental values for the proton and neutron m.m.'s, as well as their sum, which corresponds to the m.m. of an S-wave deuteron. The experimental values of the $A = 2$–3 m.m.'s have been utilized to fix the LECs, therefore predictions are for $A > 3$ nuclei. The blue dots

---

[1]Electromagnetic moments of lithium isotopes have been most recently measured in Refs. [19, 20]. At the present time, the tables and figures of this contribution and the preprint of Ref. [1] show, for these nuclei, the experimental data taken from Refs. [17, 18].
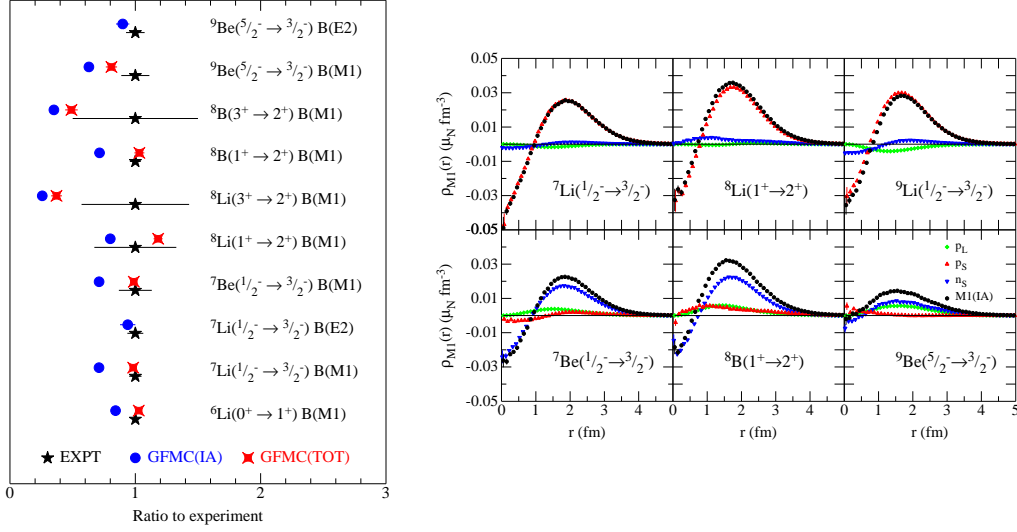
**Figure 3: Left**: Ratio to the experimental $M1$ and $E2$ transition widths in $A \leq 9$ nuclei. Black stars with error bars indicate the experimental values [17, 18], while blue dots (red diamonds) represent GFMC calculations which include the IA one-body EM current (total $\chi$EFT current up to N3LO). **Right**: $M1$ transition density in nuclear magnetons per fm$^3$ for selected nuclei, including only the IA current contribution.

labeled as GFMC(IA) represent IA theoretical predictions. The GFMC(IA) results reproduce the bulk properties of the m.m.'s of the light nuclei considered here. In particular, we can recognize three classes of nuclei, that is nuclei whose m.m.'s are driven by an unpaired valence proton, or neutron, or 'deuteron cluster' inside the nucleus. This behavior can be appreciated by looking at the IA magnetic densities represented in the right panel of Fig. 2, where the red upward-pointing triangles are the contribution from the proton spin, $\mu_p[\rho_{p\uparrow}(r) - \rho_{p\downarrow}(r)]$, and similarly the blue downward-pointing triangles are the contribution from the neutron spin. The green diamonds are the proton orbital (convection current) contribution, and the black circles are the sum. For example, we can see that the m.m.'s of $^7$Li and $^9$Li are driven by the unpaired proton, while the m.m. of $^8$Li it is due to a combined effect of the unpaired neutron acting against the proton.

In the left panel of Fig. 2, predictions, which include all the $\chi$EFT EM current contributions illustrated in Fig. 1, are represented by the red diamonds labeled GFMC(TOT). In all of the cases considered here—except for $^6$Li and $^9$Be for which the IA results are already in very good agreement with the experimental data, the predicted m.m.'s are closer to the experimental data when the MEC corrections are added to the IA results. MEC corrections are particularly pronounced in the isovector combination of the $A = 9$, $T = 3/2$ nuclei's m.m.'s, for which the MEC SNPA ($\chi$EFT) correction provides $\sim 20\%$ ($\sim 30\%$) of the total calculated isovector contribution. While the SNPA and $\chi$EFT models are in a reasonable good agreement when predicting the isovector m.m.'s—which are driven by the long-range NLO OPE contribution, we find that isoscalar m.m.'s evaluated within the $\chi$EFT model are usually in a better agreement with the experimental data [1].

In the left panel of Fig. 3, we show EM transitions induced by the M1 and E2 operators in $A \leq 9$ nuclei—E2 transitions are provided in IA only. In this figure, we show the ratios to the experimental values of the widths [17, 18]. The latter are represented with the black stars along with the associated experimental error bars, while the GFMC(IA) and GFMC(TOT) predictions are

again represented by blue dots and red diamonds, respectively. For the M1 transition in IA, we also provide their transition densities which are illustrated in the right panel of Fig. 3. As before, the red upward-pointing triangles are the contribution from the proton spin term, the blue downward-pointing triangles are from the neutron spin, the green diamonds are from the proton orbital term, and the black circles are the total IA contribution. For example, for the lithium isotopes, the M1 IA transitions are predominantly from the proton spin term, *i.e.*, these are almost pure proton spin-flip transitions. While, for $^7$Be and $^8$B, the neutron spin term is the most important, but with some contribution from the proton spin and orbital terms. The M1 results summarized in the left panel of Fig. 3, indicate that, also for these observables, predictions which account for MEC corrections are closer to the experimental values, but for the transition in $^8$Li, for which the experimental error is large, we cannot determine whether the GFMC(TOT) prediction is a better one.

## References

[1] S. Pastore, S. C. Pieper, R. Schiavilla, and R. B. Wiringa, arXiv:1212.3375.

[2] R. B. Wiringa, V. G. J. Stoks, and R. Schiavilla, Phys. Rev. C **51**, 38 (1995).

[3] S. C. Pieper, AIP Conf. Proc. **1011**, 143 (2008).

[4] L. E. Marcucci, M. Viviani, R. Schiavilla, A. Kievsky, and S. Rosati, Phys. Rev. C **72**, 014001 (2005).

[5] L. E. Marcucci, M. Pervin, S. C. Pieper, R. Schiavilla, and R. B. Wiringa, Phys. Rev. C **78**, 065501 (2008).

[6] S. Pastore, R. Schiavilla, and J.L. Goity, Phys. Rev. C **78**, 064002 (2008).

[7] S. Pastore, L. Girlanda, R. Schiavilla, M. Viviani, and R. B. Wiringa, Phys. Rev. C **80**, 034004 (2009).

[8] M. Piarulli, L. Girlanda, L.E. Marcucci, S. Pastore, R. Schiavilla, and M. Viviani, to appear on Phys. Rev. C, arXiv:1212.1105.

[9] M. Pervin, S. C. Pieper, and R. B. Wiringa, Phys. Rev. C **76**, 064319 (2007).

[10] T.-S. Park, D.-P. Min, and M. Rho, Nucl. Phys. **A596**, 515 (1996).

[11] S. Kölling, E. Epelbaum, H. Krebs, U.-G. Meissner, Phys. Rev. **C80**, 045502 (2009).

[12] S. Kölling, E. Epelbaum, H. Krebs, and U.-G. Meissner, Phys. Rev. C **84**, 054008 (2011).

[13] Y.-H. Song, R. Lazauskas, T.-S. Park, and D.-P. Min Phys. Lett. B 656, 174 (2007).

[14] Y.-H. Song, R. Lazauskas, and T.-S. Park, Phys. Rev. C 79, 064002 (2009).

[15] R. Lazauskas, Y.-H. Song, and T.-S. Park, Phys. Rev. C 83, 034006 (2011).

[16] D.R. Entem and R. Machleidt, Phys. Rev. C **68**, 041001 (2003); R. Machleidt and D.R. Entem, Phys. Rep. **503**, 1 (2011).

[17] D. R. Tilley, C. M. Cheves, J. L. Godwin, G. M. Hale, H. M. Hofmann, J. H. Kelley, C. G. Sheu, and H. R. Weller, Nucl. Phys. A **708**, 3 (2002).

[18] D. R. Tilley, J. H. Kelley, J. L. Godwin, D. J. Millener, J. E. Purcell, C. G. Sheu, and H. R. Weller, Nucl. Phys. A **745**, 155 (2004).

[19] D. Borremans *et al.*, Phys. Rev. C **72**, 044309 (2005).

[20] R. Neugart *et al.*, Phys. Rev. Lett. 101, 132502 (2008).